Macromolecules

pubs.acs.org/Macromolecules

Article

Modeling of Poly(3-hexylthiophene) and Its Oligomer's Structure and Thermal Behavior with Different Force Fields: Insights into the Phase Transitions of Semiconducting Polymers

Mosè Casalegno,* Antonino Famulari, and Stefano Valdo Meille*

Cite This: *Macromolecules* 2022, 55, 2398–2412

Read Online

ACCESS | Metrics & More | Article Recommendations | Supporting Information

ABSTRACT: The polymorphism of poly(3-hexylthiophene) (P3HT), one of the reference systems in fundamental studies of polymer semiconductors, is explored by molecular dynamics modeling of selected 3-hexylthiophene (3HT) oligomers, comparing structural and thermal behavior simulation results with rare monodisperse oligomer experimental data. The relative stability of the two crystalline polymorphs and the mechanism of interconversion between them, as the degree of polymerization grows in $(3HT)_n$ oligomers (n = 10, 16, 20) to the polymer, can be investigated in infinite periodic oligomer crystals without implicitly imposing infinite molecular weights, as inevitable for polymers. To evaluate the impact of different descriptions of molecular interactions, simulations were performed by using three different force fields specifically adapted to poly(3-alkylthiophenes) (P3ATs). Our results show that MD may adequately describe the key features and relative stability of the different crystal phases and suggest plausible interconversion mechanisms for very rapid solid−solid or melting transitions, albeit with complementary differences among different force fields, which become substantial modeling highly disordered crystal structures or mesophases.

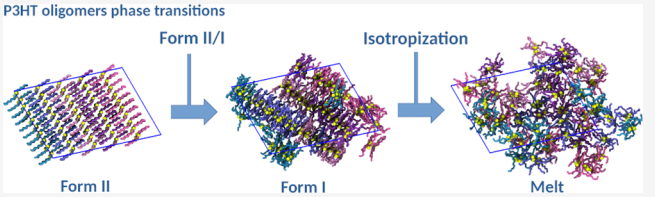

INTRODUCTION

The solid-state organization of conjugated semiconducting polymers and their complex structural dynamics represent the foundation on which efforts to improve our understanding of the physical properties of these key materials are based. The detailed characterization of the structure and of the morphology of these materials is known to be, for multiple reasons, extremely challenging while their chemical structure variety and complexity are increasing constantly due to intensive synthetic efforts to improve intrinsic molecular properties, along with attempts to optimize device performance by blending or by doping semiconducting polymers with other appropriate species. This situation is leading to intensive use of materials modeling approaches, especially MD, also for molecular systems for which very limited experimental evidence is available to validate or question the modeling results. For this reason, we believe that it is very important to use the full wealth of available experimental evidence, in the limited cases where it is available, to test and possibly validate different modeling approaches.

Poly(3-*n*-hexylthiophene) (P3HT) represents one of the most studied p-type semiconducting polymers.[1−3] In recent years it has become the reference[4−6] if not the paradigm to evaluate our understanding of these materials. Even if new semiconducting polymers are constantly being developed, P3HT, due to its high carrier mobility, good flexibility, affordable fabrication, and low-temperature solution processability, is still widely employed, often in combination with n-type counterparts,[7,8] in the study and development of organic solar cells (OSCs)[9] and organic thin film transistors (OFETs).[10]

Like for other polymers belonging to the same family, the potential of P3HT as hole transporter results from electron delocalization along the polymer backbone and, in the crystalline phases, in a favorable organization of the polymer backbone chains, which involves $\pi-\pi$ stacking of thiophene rings of adjacent stacked chains. Although, in principle, high charge mobilities can be approached,[11,12] in practice, the effective mobility is thought to be limited by local ordering and molecular packing efficiency.[13−15] While several studies have shown that carrier mobility increases with molecular weight,[13,16] the structural characterization of high molecular mass samples has proven very challenging,[17−22] as such P3HT samples consist of amorphous and crystalline domains. For the latter, a variety of supramolecular assemblies and morphologies, depending on sample properties and casting conditions,[23] have been proposed.[23,24] However, diffraction patterns obtained by different investigators indicate that crystal structures of P3HT and other poly(3-alkylthiophenes) can

Received: January 19, 2022
Revised: March 17, 2022
Published: March 31, 2022

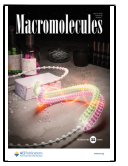

https://doi.org/10.1021/acs.macromol.2c00131
Macromolecules 2022, 55, 2398−2412

be grouped essentially in two families, characterized by either noninterdigitated (form I) or interdigitated (form II) side chains.[25−27] Form I structures present already at room temperature substantial side-chain disorder, which however increases substantially above 350 K.

The importance of P3HT and the relevance of its structural organization, dynamics, and thermal behavior are highlighted in a number of important contributions.[28−32] Particularly relevant, for this study, is the effort, by Heeney, Smith, and Koch, to synthesize[29] and characterize[30] precisely defined regioregular $(3HT)_n$ oligomers with n = 4−36 to extrapolate properties like the equilibrium melting temperatures and melting enthalpies of different crystalline phases of P3HT, and hopefully its ultimate mechanical and electronic properties, avoiding issues like molecular mass dispersity and segregation, entanglements, and chain folding. Furthermore, precisely defined oligomers are normally easier to crystallize[32] and therefore better suited to study the thermodynamic stability of different crystalline phases. Indeed, ref 30 reports a wealth of experimental information that represents a very challenging benchmark to evaluate our ability to model semiconducting polymers and oligomers. The mentioned paper convincingly shows that the diffraction patterns of $(3HT)_n$ oligomers, for n > 9 are extremely close to those of well-crystallized P3HT, albeit as expected better resolved, indicating that the structural families of these oligomers closely correspond to the polymer's polymorphs. Similar conclusions are reached by spectroscopic approaches.[33] The paper by Koch et al.[30] also clearly indicates that form I crystal structures are more difficult to obtain and present a lower meting point as compared to form II structures, for $(3HT)_n$ oligomers, up to n = 12. As apparent in Figure 1, based on data from ref 30, above that degree of

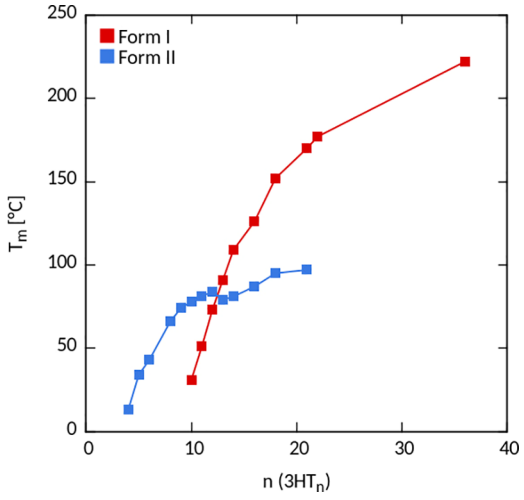

Figure 1. Experimental melting points of the two crystalline modifications in which $(3HT)_n$ oligomers crystallize as a function of the degree of polymerization n. Data are reported with permission from ref 30.

polymerization, form II becomes the lower melting polymorph, even if its melting enthalpy per monomer remains between 2 and 3 times the melting enthalpy of form I, because of lower internal energy, associated with higher density and to a more efficient crystal packing. Form I is the fast-forming, more easily accessible, entropy-stabilized polymorph typically observed in long 3HT oligomers and polymers.[27,30,34−36] At room temperature, for n > 10, the two polymorphs may coexist, depending on processing conditions and thermal history. The conversion of one form into the other is possible, and the form II−form I transition is suggested[30] to occur in the case of oligomers by melting/recrystallization. As apparent in Figure 1 for $(3HT)_n$ oligomers, from n = 13 form I becomes the higher melting modification, as found for P3HT. The form II−form I transition, as temperature increases, has been indeed experimentally documented for P3HT and for other poly(3-n-alkylthiophenes) (P3ATs),[35,36] although in the case of polymers a solid−solid transition has been proposed.[37] It is interesting to point out that the degree-of-polymerization-dependent "crossover" of the melting points of two phases, apparent in Figure 1, mirrors a general behavior described for oligomer systems displaying a mesomorphic phase along with a crystalline phase,[38] the mesophase being virtual or monotropic for low DP and becoming increasingly stable with increasing DP for entropic reasons. This suggests a broader perspective for our understanding of the interplay between form I and form II in P3ATs.

We have recently shown that standard, unbiased MD can be applied to the study of form II−form I phase transition in the case of P3AT polymers. Our study[39] was able to evidence a fast, solid-state transition giving new insight into the structural reorganization which occurs and in the type of disorder to be expected in the resulting form I. On the other hand, while the facts that for P3HT the transition is observed at a significantly lower temperature than for poly(3-n-butylthiophene) (P3BT) and that for both crystal forms P3BT presents higher melting points than P3HT are correctly represented in our work; the temperatures at which the form II−form I transitions occur and the melting temperatures of the two polymorphs were in all the studied cases estimated to be about 200 K higher than the experimental values. These large, somewhat discouraging deviations could be due to various reasons, among which the most relevant are the infinite molecular weight and the extended-chain morphology implied by the infinitely periodic crystals assumed in our MD simulations, but we should not forget the possibility of disorder, small size, and defects in experimental crystals of the lower melting form II. The infinite lateral crystal dimensions in simulations could also be relevant as well as the features and limits of the adopted force field. Indeed, as we will see in this study, also the choice of the force field can have a great impact on the simulation results due to the delicate balance between inter- and intramolecular interactions in these systems.

To clarify these issues and to better evaluate the general reliability of the insights resulting from simulation studies, we decided to expand our work along two directions that we consider of major relevance. The first it to check whether other force fields, especially developed for P3ATs and already reported in the literature, can adequately model the form II−form I transition in the case of P3HT. While continuing to work with the force field used in our initial study,[39−41] we selected two additional force fields[42−44] to determine how well results with different force fields reproduce experimental data and how the different modeling results compare. The second endeavor was investigating by MD approaches, using the three force fields, the behavior of $(3HT)_n$ oligomers, whose experimental behavior we discussed above. Although MD studies of crystalline $(3HT)_n$ oligomers also involve infinitely periodic crystals, the problem of infinite molecular weight, present in our infinitely periodic polymer crystal studies, is suppressed, making evaluations easier. Indeed transitions

https://doi.org/10.1021/acs.macromol.2c00131
Macromolecules 2022, 55, 2398−2412

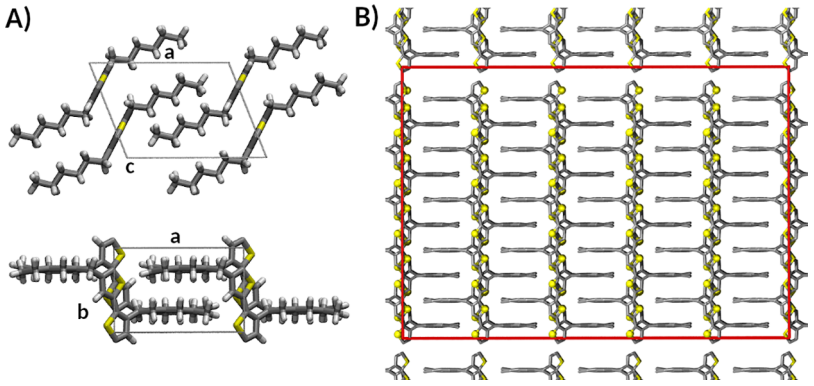

Figure 2. (A) Crystal structures of P3HT form II adopted in this work. Unit cells are highlighted in blue. Hydrogen atoms have been omitted for clarity. (B) Sketch of a $(3HT)_{10}$ supercell in the initial configuration. The cell boundaries are highlighted in red. Hydrogens have been omitted for clarity.

involving $(3HT)_n$ oligomer crystals appear a particularly sound and challenging testing ground, even if the available experimental structural data also for these systems are quite limited.

We conclude our introductory remarks listing some questions that we can hopefully contribute to answer in the present work: (i) What are the molecular factors responsible for the stability of a given polymorph for different oligomer lengths in $(3HT)_n$ systems? (ii) What are the mechanisms underlying the form II−form I conversion, and why does the latter only take place in relatively long oligomers and polymers? (iii) Is the form II−form I conversion mechanism identical for oligomers and polymers? This all leads to the key question that lies at the root of most of our recent investigations: to what degree can we expect the structural models derived from MD simulations to be reliable, as a function of temperature, for P3AT's and other conjugated polymers? Our findings and their impact on the ongoing debate on P3HT structural organization are discussed in light of the available literature.

SYSTEM SETUP

As the starting point for the MD simulations, we considered perfect, defect-free form II crystals made up of 3HT chains, either polymeric (P3HT) or $(3HT)_n$ oligomers formed by n monomers. All simulation boxes were assembled starting from the polymer form II unit cell (space group $P2_1/c$) containing two chains depicted in Figure 2, with the following lattice parameters: a = 12.9 Å, b = 7.8 Å (chain axis), c = 9.44 Å, and β = 68.40°, taken from our previous work.[39]

For the polymer system, the supercell was built replicating the unit cell 5 times along all axes so as to obtain 50 chains, each consisting of 10 monomers. The chains are effectively infinite since they are connected head-to-tail across the periodic boundaries. Periodic boundary conditions were applied along all lattice directions.

Because no detailed form II crystal structures are available in the literature for $(3HT)_n$ oligomers, sensible models had to be generated considering the available experimental evidence. The initial values for a, c, and β, but also α and γ, were assumed to be identical with P3HT form II values, in agreement with published work by Rahimi et al.[32] The other main guideline was the consideration that powder diffraction patterns obtained from oligomers adopting form II, especially from $(3HT)_{10}$ upward, are very similar to P3HT form II patterns and increasingly so as the degree of polymerization grows.[30] Another important indication was the absence of even/odd effects in the oligomer crystal structures.[30] It was hence attempted to keep changes with respect to the polymer unit cell at a minimum, essentially imposing translational repetition after one molecule in the main chain direction (i.e., the b-axis). This was simply achieved reducing the symmetry, which amounts to adopting the P-1 space group, since the 2_1 symmetry with 7.8 Å axial periodicity of the main chain is lost. Initial values for b in the case of oligomers were obtained from simple geometrical considerations ($b \approx (n{\cdot}3.9 + \text{const})$ Å) and from values observed for axial periodicities in the crystalline oligomers.[30] The constant represents the additional spatial requirement along the main chain axis to avoid intermolecular atomic clashes and has an approximate value of about 2.2 Å. The chain ends were capped with hydrogen atoms.

Oligomers' supercells were generated following an approach similar to that for P3HT. The number of unit cell replicas along a and c was kept fixed at 5. The starting b-axis value of the supercell, coinciding with main-chain axis direction, was set to correspond to its preliminarily estimated value for the unit cell of the specific oligomer, i.e., about 41.2, 64.6, and 80.2 Å for $(3HT)_n$ with n = 10, 16, and 20, respectively. An example of oligomer supercell is given in Figure 2B for $(3HT)_{10}$. Periodic boundary conditions were applied so as to simulate an infinite periodic crystal.

FORCE-FIELD SELECTION

It is well established that the choice of the force field has a significant impact on the calculation of the structural and thermodynamic properties of P3HT and related compounds.[45] For this reason, among the force fields that are currently available,[46−54] we focused on three that were specifically developed to describe the dynamics of 3HT compounds (see below). As a preliminary consideration, we note that these force fields can be expected to perform better than general purpose ones,[46,47] which have in some cases also been adopted to model P3HT systems.[55] Coarse-grained force fields[52,53] were excluded as well, since they are typically targeted toward disordered states (melts, blends, solutions, and glasses), and we are not aware of any proof that they can deal with crystalline states and their transitions. We further note that our selection includes only force fields that were extensively validated against experimental data, such as crystal structures, densities, melting

https://doi.org/10.1021/acs.macromol.2c00131
Macromolecules 2022, 55, 2398−2412

temperatures, persistence lengths, and end-to-end lengths in long thiophene oligomers.

Finally, particular attention was also paid to the approaches used to assign the atomic partial charges and the backbone torsional potential, as those parameters were found to have the greatest impact on solid state structure and dynamics.[45]

Based on the above criteria, the following force fields were selected: (1) the force field developed by Moreno et al.[40,41] (third parameter set), hereafter abbreviated as FF3; (2) the force field developed by Bhatta et al.,[42,43] hereafter abbreviated as BHA; (3) the OPLS-compatible force field proposed by Wildman et al.,[44] hereafter abbreviated as OPL.

FF3 is one of the three force fields developed by our group aimed at describing both 3HT polymers and oligomers. The atomic charges were derived from B3LYP/6-311G** charge distributions by an empirical correction, whereas torsional potentials were obtained at the same level of theory by scanning the potential energy surfaces of tetrathiophene. Its reliability was tested against the crystal structures of 11 oligomers. The choice of this force field is essential since the present investigation is an expansion to oligomers of our recent study[39] of the form II−form I transition involving P3HT and P3BT (i.e., poly(3-*n*-butylthiophene)) which proved possible by using FF3.

BHA was specifically developed to describe the P3HT solid-state behavior. Partial atomic charges were obtained via the RESP[56,57] approach, at the MP2/6-31+G(d,p) level, while for torsional parameters a DFT level using the B3LYP functional was preferred. This force field was successfully tested against P3HT packing motifs and melting temperature. Minor modifications of the BHA force field, involving essentially terminal thiophene units, were required to deal with oligomer structures. These are detailed in the Supporting Information.

For OPL also, the last examined force field, the atomic charges were obtained by the RESP scheme using as input the DFT (CAM-B3LYP/cc-pVTZ) electronic densities. Torsional parameters were obtained by using a scanning approach, resembling that used for FF3, albeit with a different DFT functional (CAM-B3LYP/6-31G*). This FF was developed to describe P3HT, however not explicitly in the solid state, and was validated by showing it provides persistence lengths and end-to-end distributions consistent with experimental values for long 3HT oligomers.

It is important to note that all the FF have a common origin in the OPLS-AA parametrization.[48−51]

In all FF, Lennard-Jones parameters were essentially left unchanged with respect to the original parametrization. However, considering the importance of partial atomic charges in describing system dynamics, we can say that the FF considered have relatively little resemblance with their parent force field, whose validity has recently been questioned.[55]

SIMULATION DETAILS

Full atomistic simulations were performed with the package Gromacs 2020.[58−60] The equations of motion were propagated with a leapfrog algorithm with a time step of 1 fs. All simulations were performed within the NPT ensemble. The system temperature was kept constant via the velocity rescaling algorithm developed by Bussi et al.,[61] with a time constant of 0.5 ps.

The choice of the barostat was made after some preliminary tests. Because of its sensitivity to large box deformations, the Parrinello−Rahman (PR) barostat[62] was used in production runs not involving phase transitions. The Berendsen barostat,[63] conversely, was used to perform equilibration runs and all the runs aimed at detecting a phase transition. For both barostats, the coupling time constant was set at 5.0 ps and isothermal compressibility at 1×10^{-6} atm^{-1}. The electrostatic interactions were treated via the particle-mesh-Ewald method[64] with a Fourier grid spacing of 0.12 nm. The same cutoff was used also for the truncation of the Lennard-Jones interactions.

All supercells were initially equilibrated (20 ns) at constant pressure (1 atm) and temperature (300 K). The same simulation parameters were used to perform production runs, with variable simulation times (up to 80 ns). This upper limit was chosen based on our previous work on P3AT disordering transitions[39] (see particularly the Supporting Information to ref 39) where it was found that 80 ns exceeded typically by a factor larger than 2 the time required to complete either the form II−form I transition or the form II isotropization at all investigated temperatures where the transitions did occur.

The trajectories were further postprocessed and analyzed with a suite of programs developed in our group.

For comparison purposes, DFT calculations were also performed on the polymer form II unit cell with the package DMol3.[65] The electron density associated with the molecular orbitals was expanded by means of a numerical double-ζ quality basis set, including polarization functions on all atoms (i.e., DNP), roughly comparable to the 6-31G** set. The Perdew−Burke−Ernzerhof (PBE)[66,67] functional was adopted in all calculations. The van der Waals terms were explicitly included to describe dispersion interactions.[68,69] Energy minimizations were performed allowing relaxation of unit cell parameters and atomic coordinates. Graphics and figures have been produced by means of the following programs: VMD,[70] Gnuplot,[71] and Discovery Studio.[72]

RESULTS AND DISCUSSION

Force-Field Testing against Experimental and DFT Form II P3HT and Oligomer Lattice Models. During the early stages of our work, we performed calculations aimed at obtaining information about the descriptive ability of the adopted force fields. To this end, we optimized the atomic positions and the unit cell parameters by minimizing the potential energy associated with the different force fields for the polymer form II unit cell (see Figure 1a). For comparison purposes, energy minimization on the same unit cell was also performed at the DFT level. All force field minimizations were performed by using an in-house program developed to optimize atom coordinates and unit cell parameters under the symmetry constraints imposed by a given space group. In this case, periodic boundary conditions were imposed on all axes, and the space group was constrained to $P2_1/c$.

Table 1 summarizes the results of these calculations. The starting values were obtained as explained in ref 39 by using force field FF3. As compared to the starting parameters values, all force fields exhibited marginal increase of the *a*- and *b*-axis and a decrease of the *c*-axis. For FF3, the small resulting differences can be ascribed to the use of minimization algorithms different from those adopted in previous work.[39] The energy-minimized lattice parameters were comparatively larger than those obtained by means of DFT calculations. This outcome was expected, as the descriptions offered by force fields are typically thought to underestimate intermolecular interactions, thus resulting in unit cells with lower density than values obtained at the DFT level.

https://doi.org/10.1021/acs.macromol.2c00131
Macromolecules 2022, 55, 2398−2412

Table 1. Unit Cell Parameters and Densities Resulting from Energy Minimization of P3HT Form II Unit Cell

parameter	starting values[a]	FF3	BHA	OPL	DFT
density (g/cm^3)	1.250	1.244	1.247	1.249	1.416
a (Å)	12.90	12.987	12.994	12.940	12.660
b (Å)	7.80	7.811	7.870	7.915	7.796
c (Å)	9.44	9.410	9.315	9.284	8.510
α (deg)	90.00	90.00	90.00	90.00	90.00
β (deg)	68.40	68.40	68.40	68.40	68.17
γ (deg)	90.0	90.00	90.00	90.0	90.00

[a]See ref 39.

Of particular interest is the contraction of the c-axis, which identifies the direction of the main-chain stacking. The distance between the planes of adjacent chains along this direction is 3.95 Å (c sin β) for DFT but increases to about 4.35 Å regardless of the FF considered. No change was observed in the unit cell angles, whereas for the DFT treatment, a minor reduction of β was observed. Notwithstanding the differences, these calculations confirmed that the form II structure was a stable energy minimum for all the three force fields considered.

The form II lattices developed for $(3HT)_{10}$ and $(3HT)_{16}$ were also tested with DFT calculations showing these interdigitated structures (see the Supporting Information, Table S9) to be well-defined, stable minima, albeit unsurprisingly with differences with respect to lattices optimized with MD at room temperature (see below). The lattice energy per monomer increases from 95.5 kJ/mol for $(3HT)_{10}$ to 95.9 kJ/mol for $(3HT)_{16}$ and to 99.0 kJ/mol for the polymer form II structure, suggesting a mild increment with the degree of polymerization. There is hence evidence of a modest destabilization due to the terminal groups, supporting our extrapolation of the form II oligomer crystal structures from the polymer lattice.

As a next step, we simulated the dynamics of P3HT at 300 K for 40 ns. Table 2 summarizes the results of the MD simulations. The calculated average densities at this temperature well agree with the experimental values of 1.14−1.16 g/cm^3.

Table 2. Average Values of the Density and the Unit Cell Parameters for P3HT at 300 K[a]

parameter	FF3	BHA	OPL
density (g/cm^3)	1.196 ± 0.003	1.176 ± 0.004	1.197 ± 0.001
a (Å)	13.288 ± 0.033	13.417 ± 0.047	13.474 ± 0.036
b (Å)	7.814 ± 0.007	7.851 ± 0.015	7.918 ± 0.089
c (Å)	9.355 ± 0.028	9.358 ± 0.042	9.089 ± 0.025
α (deg)	90.0 ± 0.7	90.0 ± 3.8	90.0 ± 0.7
β (deg)	72.0 ± 0.2	72.8 ± 0.2	72.1 ± 0.2
γ (deg)	90.0 ± 0.7	90.0 ± 2.4	90.0 ± 0. 5

[a]All the values reported were obtained by appropriately rescaling supercell parameters.

Interestingly, thermal relaxation resulted in all force fields in an increase of the cell size along a, a slight increase in the β angle, and a contraction of the c (stacking axis) length. The standard deviations of the cell parameters indicate the simulated systems are stable at room temperature. Although the simulated systems imply an infinite chain length, a tentative comparison with literature data can be made with the values obtained by Rahimi et al.[32] for P3HT with relatively low molecular weight (a = 13.1 Å, c = 9.3 Å, and β = 68.5°) and adopting for the intrachain chain periodicity (b-axis) the value of 7.80 Å, obtained from the DFT calculations. Deviations from experimental values in the case of the OPL force field are somewhat larger than with FF3 and BHA.

Force-Field Testing: Simulated Form II $(3HT)_n$ Diffraction at 300 K against Experimental Data. Given these preliminary results for polymeric form II structures, we evaluated the performance of the three force fields modeling the $(3HT)_n$ oligomers (with n = 10, n = 16, and n = 20) structure. All oligomer supercells were first equilibrated at room temperature. The cell parameters obtained from the NPT production runs (40 ns), using the PR barostat, at this temperature are reported in the Supporting Information.

To compare the results of these simulations with the data available in the literature, we report in Figure 3 the calculated XRD spectra obtained for the $(3HT)_{10}$ and the $(3HT)_{16}$ oligomers in the form II modification, as modeled adopting the three different force fields. In Figure 3, experimental form II diffraction patterns for the two oligomers are also reproduced from ref 30.

In the region with 25 > q > 4 nm^{-1} the diffraction patterns in Figure 3 are unsurprisingly dominated by the contribution of the $h0l$ reflections, which are the equatorial reflections taking b as the main-chain axis for consistency with the adopted P3HT lattice (Table 1). The $h0l$ reflections indexing of the diffraction patterns is straightforward, and clearly consistent also with respect to intensities, with the equatorial P3HT form II equatorial electron diffraction patterns.[32] We observe that, indeed, equatorial reflections are often the most intense in polymer crystal structures. Because the projection of the form II crystal structure along the chain axis is nearly identical for all $(3HT)_n$ oligomers from n = 10 up to the polymer, it becomes readily understandable why all of them show very similar experimental X-ray diffraction data,[30] the main varying feature being the increased broadness (FWHM) of the diffraction maxima,[30] largely due to increasing crystallization difficulty and smaller crystallites with increasing molecular mass. The other experimental diffraction pattern differences, varying the degree of polymerization, concentrate in the region between the 202 and the 302 reflections, i.e., roughly in the range with 15 < q < 17 nm^{-1}, where some of the more intense nonequatorial reflections occur.

The diffraction patterns calculated from form II structures obtained with the three force fields in the region 25 > q > 4 nm^{-1} are for a given oligomer, rather similar in the sense that the more intense reflections are in essence the same, although the q values may differ because of the differences in the lattice parameters optimized with the three force fields (see Tables S2−S4). If the lattice parameters were fixed, e.g., at their experimental values at 300 K, diffraction pattern differences in the q range 4−25 nm^{-1} would plausibly be quite small. As we observed for experimental patterns, differences among the calculated patterns for the $(3HT)_{10}$ and the $(3HT)_{16}$ oligomers, with structures obtained with all three force fields, are most apparent in the region between the 202 and the 302 reflections, where intense nonequatorial reflections occur: this is reasonable, mainly because of the different value of the molecular length and hence of the b-axis but more in general because the details of calculated 3D crystal structures plausibly differ more than their projections along the molecular axis.

https://doi.org/10.1021/acs.macromol.2c00131
Macromolecules 2022, 55, 2398−2412

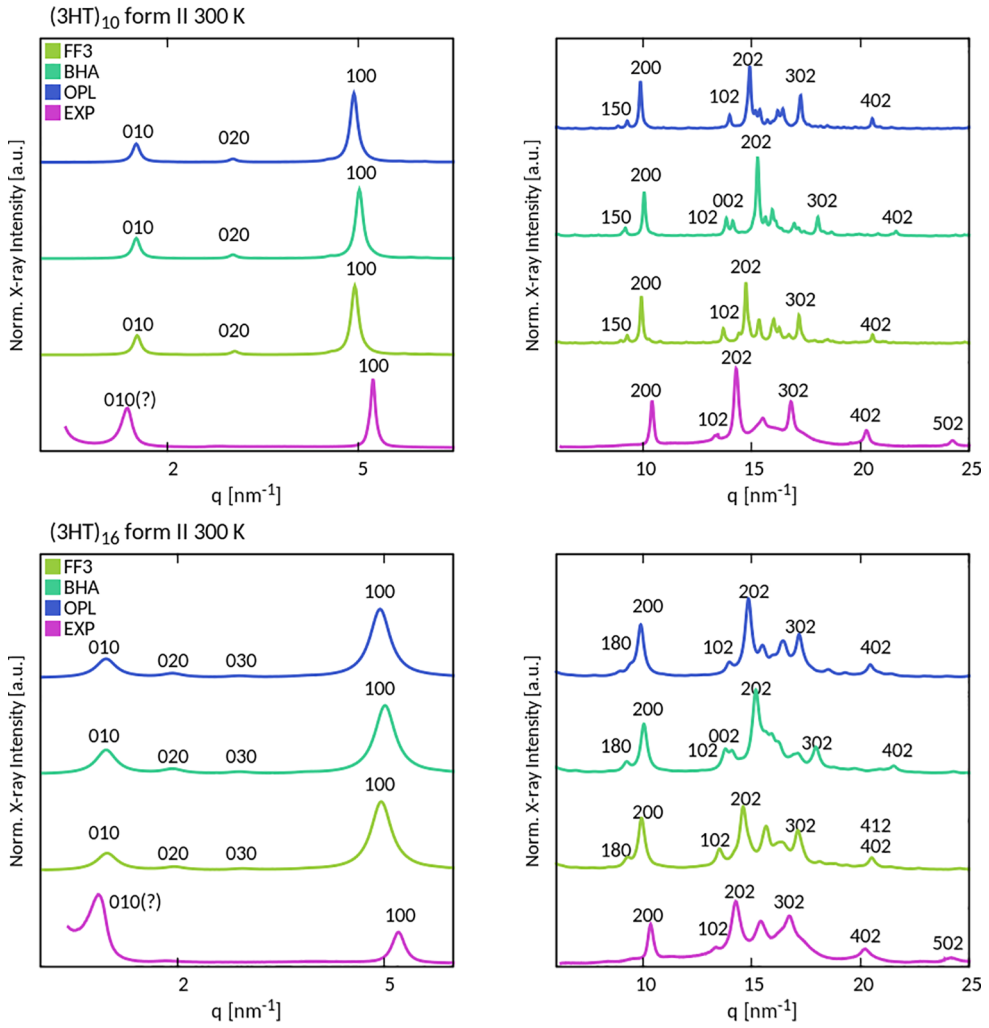

Figure 3. XRD patterns calculated for the form II $(3HT)_{10}$ (above) and the $(3HT)_{16}$ oligomer (below), modeled with the three investigated force fields at 300 K. The experimental form II diffraction patterns for the two oligomers are also reproduced (with authors' permission) from ref 30. Low and high q data are shown side by side in separate panels because experimental data were recorded[30] with two different detectors. The shown indices refer to the two-chain unit cell reported in Tables S2−S4 for the oligomers. For the $h0l$ reflections, indices correspond essentially with those resulting if the polymer unit cell is adopted.

Notice in this respect that for the $(3HT)_{10}$ and the $(3HT)_{16}$ oligomers, with structures obtained with all three force fields, non-negligible nonequatorial 150 and 180 reflections, respectively, are calculated in a different region, namely at q values just below the 200 reflection. Because such non-equatorial reflections are absent in experimental patterns, this fact suggests some overestimation of 3D order in the case of the form II structures calculated with all three force fields.

Differences in the diffraction patterns of different oligomers are apparent in Figure 3 in the $q < 4$ nm^{-1} range, where the lower order $0k0$ diffraction maxima occur, related to the main-chain periodicity of the oligomers, described as aligned along the b-axis in the present paper. This region of the calculated patterns, in the case of each oligomer, are essentially superimposable for structures calculated with the three different force fields. They, however, differ from the experimental patterns because the reflection indexed as 010 is substantially more intense as compared to the 100 reflection in the experimental than in calculated patterns, which in turn clearly show also the 020 reflection and, for the longer $(3HT)_n$ oligomers with n = 16 and 20, also the 030, all of which are experimentally negligible. Another discrepancy should be mentioned: in the case $(3HT)_n$ with n = 10 the experimental value of the d-spacing of the form II reflection indexed tentatively as 010 is about 4.58 nm, i.e., about 5 Å greater than expectations based on the molecular length. For $(3HT)_n$ with n = 16 the form II experimental reflection with tentative indices 010 shows a d-spacing value of 7.5 nm, 10 Å greater than the 6.48 nm value in the form I $(3HT)_{16}$ structure, which closely corresponds to the value expected from the molecular length and to the form II b-axis value found for this oligomer with all three force fields.

The absence of the 020 and the 030 reflections in experimental form II patterns can be explained by higher disorder in the experimental than in the simulated structures or else by very small crystallite dimension along this direction. On the other hand, reflections which in experimental form II patterns are tentatively indexed as 010 might have a different origin: they could possibly be due to crystalline/amorphous alternation in that direction.

Modeling the Thermal Behavior and Structural Evolution of Form II P3HT. The next step in our study was the comparison of how the polymer, i.e., P3HT, form II structure evolved with increasing temperature with the three

https://doi.org/10.1021/acs.macromol.2c00131
Macromolecules 2022, 55, 2398−2412

different force fields. In the case of FF3 we confirmed[39] the already reported transition to the form I structure at 530 K. At the same temperature, adopting the BHA and the OPL force fields the form II type structure proved to be stable. We had to increase the temperature to 560 and 600 K, respectively, to observe a transition with the BHA and the OPL force fields. In both cases form II P3HT did not transform to an isotropic melt but to form I type structures as in the case of FF3. To make more meaningful comparisons, the form I structures obtained with the three force fields were cooled to the same temperature of 300 K. Figure 4 reports the final frames obtained from these simulations.

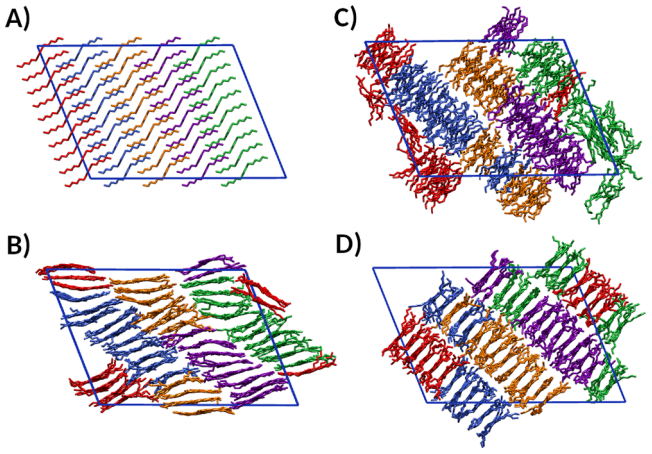

Figure 4. P3HT structures (hydrogens omitted for clarity) obtained with the different force fields: FF3 (panel B), BHA (panel C), and OPL (panel D), after the transition to form I. For comparison purposes, the starting form II frame is shown (panel A), and the original unit cell is drawn also in the final models to help the appreciation of changes. The form I structures shown are all cooled to 300 K for the sake of comparison. The original form II and final from I stacking organization are highlighted, with chains color coding according to the initial stacking.

The resulting form I structures obtained with the three different force fields show, on the one hand, similar features but also remarkable differences. The most apparent similarity is the reorganization of the form II stacks into new stacks in which blocks of the original form II are preserved. The average size of the original blocks is, however, 8.3 chains with the BHA force field, while one block of two chains is trapped between stacks and oriented very differently than the other 48 chains in the supercell. With OPL the structure is highly regular with an average block size of 4.5 chains, while with FF3 the average block size of the organized chains is 5.0. Of the 50 chains in the supercell, 6 with FF3 remain highly disordered, 4 of them (green in Figure 4) in a single group, and 2 (red in Figure 4) as individual chains, trapped between stacks. Notably with all three force fields, the new from I stacks are tilted quite similarly, by an angle of 20°−30° with respect to the original form II stacks. The different degrees of disorder in the resulting form I structures are apparent in what has just been discussed as well as on superficial inspection of Figure 4. The degree of disorder in the alkyl side chains is similar for BHA and OPL but much more extensive in the case of FF3.

The distributions of main-chain torsion angles, averaged over 40 ns (800 frames), along with those obtained from analogous runs performed on form II structures, are shown in Figure 5, for all force fields. The distributions are in all cases narrower in the case of form II, where the side-chain interdigitation locks in also the main-chain conformation. OPL distributions are also somewhat narrower than for BHA. For FF3 the distribution is comparable in the case of form II, and in fact its broadness is intermediate between BHA and OPL, whereas in the case of form I FF3 shows a bimodal distribution with maxima centered at about 40 °C on both sides of the *trans* conformation. These observations, together with the higher transition temperatures recorded with BHA and OPL, point to a much higher apparent stiffness of the P3HT chains with these force fields as compared to FF3. We will come back to this point later.

Modeling the Thermal Behavior and Structural Evolution of Form II $(3HT)_n$. To study the $(3HT)_n$ oligomers thermal behavior, we also performed for these systems MD simulations at increasing temperatures. Guided by our previous work on P3ATs phase transitions,[39] we decided to set the starting temperature for these investigations at 450 K. Independent NPT simulations were then performed in successive 40 ns runs raising the temperature by increments of 30 K. When necessary, smaller increments, down to 10 K, were also adopted to improve estimates of the transition temperatures. Starting from form II, two kind of phase transitions were observed, namely, the form II−form I conversion or the transition to an isotropic molten phase.

The phase transition temperatures for all oligomers and all force fields are reported in Tables 3 and 4. The reported temperatures were the minimum temperatures at which the corresponding phase transition was observed to occur within 40 ns. More detailed tables showing all the results of MD simulations performed at different temperatures are supplied, for each studied system, in the Supporting Information.

The first investigated oligomer is $(3HT)_{10}$, for which the experimental melting temperature of form II is 348 K. At variance with observations for higher oligomers and for the polymer, it occurs experimentally 44 K above the form I melting temperature (304 K).[29,30] On the basis of these data, we might expect form II to melt and not to convert to form I. The results of the MD simulations confirm this expectation using the FF3 and OPL force fields (see Table 4), where the phase transition to the isotropic melt was detected at 470 and 540 K, i.e., respectively, about 120 and 190 K above the experimental transition. For the BHA force field, on the other hand, starting at 560 K (210 K above the experimental temperature, see Table 3), the form II structure was observed to convert to a two-dimensional semiordered structure represented in Figure 6, having the structural features of a form I structure. With the BHA force field, the transformation for $(3HT)_{10}$ is hence similar and occurs at the same temperature at which it is observed for the polymer with infinite molecular weight. However, inspection in panel D of Figure 6 of the resulting model very interestingly shows extensive disordering of the molecules along the axial direction, so that molecular layers which existed in form II are largely lost and the remaining order is only in the projection displayed in panel C of Figure 6. The resulting form I type structure shows in other words essentially only nematic-type order, plausibly preserved by main chains acting as mesogenic groups. This result appears hardly in agreement with experimental indications[30] since, in the case of $(3HT)_{10}$, form II melts to the isotropic state at lower temperature than form I, while in the case of higher oligomers for which the solid state form II−

https://doi.org/10.1021/acs.macromol.2c00131
Macromolecules 2022, 55, 2398−2412

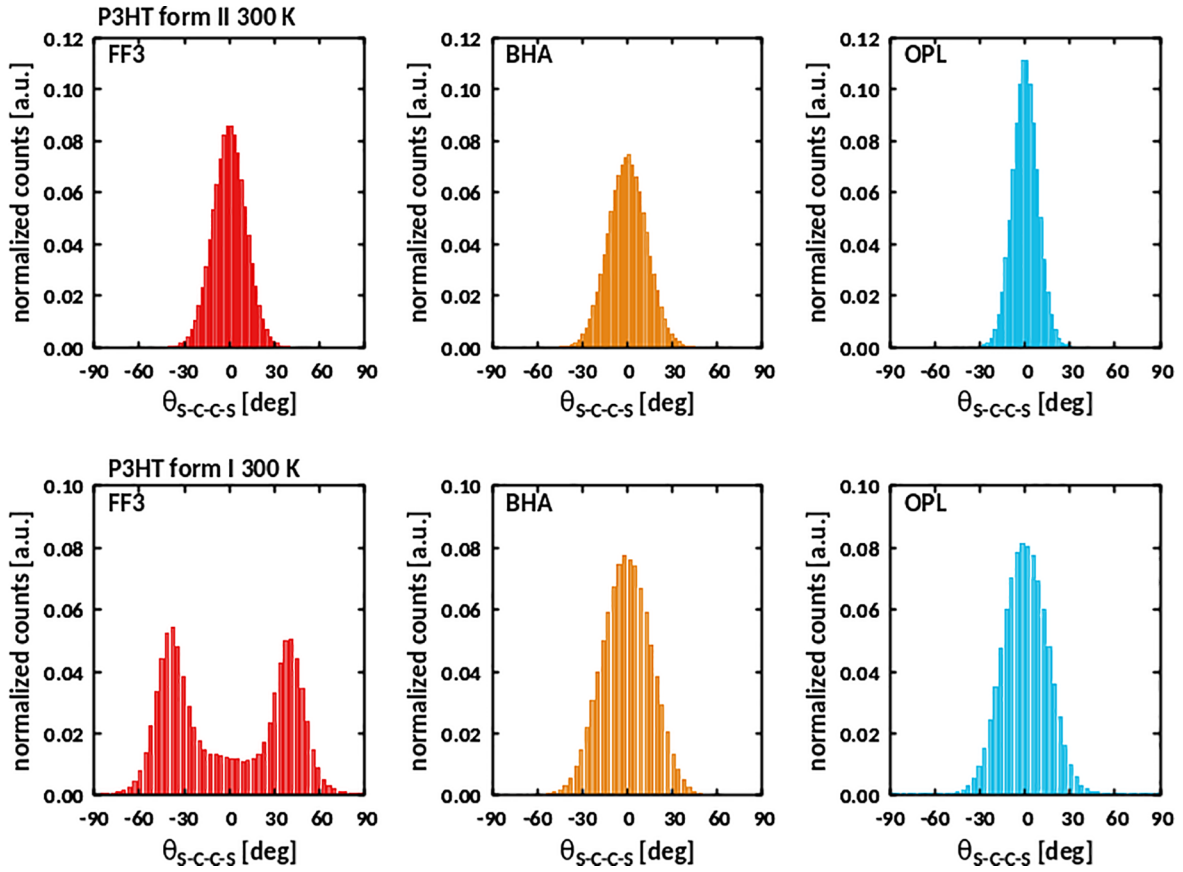

Figure 5. Distribution of main-chain dihedral angle values obtained from MD simulations at 300 K for P3HT form II (above) and form I (below). The $\theta_{S-C-C-S}$ value of 0° corresponds to the *trans* arrangement of the S atoms of adjacent monomers.

Table 3. Estimated Form II–Form I Transition Temperatures, Enthalpies, and Entropies (per Mole of 3HT Units) of the Form II Polymorphs of $(3HT)_{10}$, $(3HT)_{16}$, $(3HT)_{20}$, and "Infinite" P3HT Obtained with the Three Adopted Force Fields Compared to Available Literature[30,39] Experimental Values[a]

	FF3			BHA			OPL			expt.		
$(3HT)_n$	ΔH (kJ/mol)	ΔS (J/(K mol))	T (K)	ΔH (kJ/mol)	ΔS (J/(K mol))	T (K)	ΔH (kJ/mol)	ΔS (J/(K mol))	T (K)	ΔH (kJ/mol)	ΔS (J/(K mol))	T (K)
10				15.2	27.1[d]	560				9.0	24.1	304[b]
16				13.8	24.6[d]	560				7.3	21.4	360
20				14.0	25.0[d]	560				6.9[c]	20.7[c]	369[c]
P3HT	11.8	22.3[d]	530	13.5	24.1[d]	560	14.0	23.3[d]	600	6.8	23.6	389

[a]This transition for the studied oligomers does not occur with FF3 and OPL. [b]The experimental $(3HT)_{10}$ form I melting/form II recrystallization occurs at 304 K while the form II melting is at 351 K (Table 4). Hence, the calculated form II to form I ΔG value at 304 K is >0, and accordingly the reverse transition can be experimentally observed for this oligomer.[30] [c]Interpolated from experimental values pertaining to $(3HT)_{18}$ and $(3HT)_{21}$. [d]Values estimated, assuming equilibrium between form II and form I at the transition temperature. This is unlikely since for the solid–solid transformation to occur, form I likely has a lower free energy at the transition temperature. This ΔS values are hence likely to be underestimations.

form I transformation could in principle occur, sharp axial 010 and 020 reflections (001 and 002 according to the convention generally adopted[29]) are reported for the resulting form I.[30] These features suggest persistence, and even perfecting of layered molecular organization in stable form I oligomers structures obtained experimentally from form II, i.e., at the very least some kind of smectic-like molecular order. Hence, this axial disordering apparent with the BHA force field could possibly be interpreted as a just transient feature which experimentally is largely "annealed out" from stable form I oligomer structures.

In the case of $(3HT)_{16}$, the experimental melting temperature of form II is 360 K, a value which is 39 K lower than the reported form I melting temperature (399 K).[30] Indeed, in the case of this oligomer, form II crystals experimentally transform to form I at 360 K, with a mechanism that is speculated[30] to involve a melting–recrystallization process. The results of the MD simulations (see Table 4) for the FF3 and OPL force fields show for $(3HT)_{16}$ a phase transition to the isotropic melt at 490 and 560 K, respectively, i.e., for both these force fields, 20 K higher than in the case of $(3HT)_{10}$. In the case of $(3HT)_{20}$, the same transitions occur in MD simulations with the FF3 and OPL force fields at 500 and 580 K, respectively.

https://doi.org/10.1021/acs.macromol.2c00131
Macromolecules 2022, 55, 2398–2412

Table 4. Estimated Isotropization Temperatures, Enthalpies, and Entropies (per Mole of 3HT Units) of the Form II Polymorphs of $(3HT)_{10}$, $(3HT)_{16}$, $(3HT)_{20}$, and "Infinite" P3HT Obtained with the Three Adopted Force Fields Compared to Available Literature Experimental Values[30,39 a]

	FF3			BHA			OPL			expt.		
$(3HT)_n$	ΔH kJ/mol	ΔS J/(K mol)	T (K)	ΔH (kJ/mol)	ΔS (J/(K mol))	T (K)	ΔH kJ/mol	ΔS (J/(K mol))	T (K)	ΔH (kJ/mol)	ΔS (J/(K mol))	T (K)
10	13.8	29.4	470				19.1	36.0	530	12.5	35.6	351
16	14.1	28.8	490				21.2	38.5	550	11.5	31.9	360[c]
20	14.4	28.8	500				23.8	41.0	580	11.7[b]	31.7[b]	369[b,c]
P3HT										15.0	38.6	389[c]

[a]Direct form II isotropization does not occur for P3HT with all three force fields and, in the case of BHA, neither for the studied oligomers. [b]Interpolated from experimental values[30] pertaining to $(3HT)_{18}$ and $(3HT)_{21}$. [c]The experimental form II T_m values (Figure 1 and Table 4) and of the observed from II−form I transition temperature (Table 3) for P3HT, $(3HT)_{16}$, and $(3HT)_{20}$ are reasonably assumed to coincide. For $(3HT)_{10}$ the form II T_m is higher than for form I, and a slow form I−form II transition can be observed experimentally heating form I at the T_m of form I.[30]

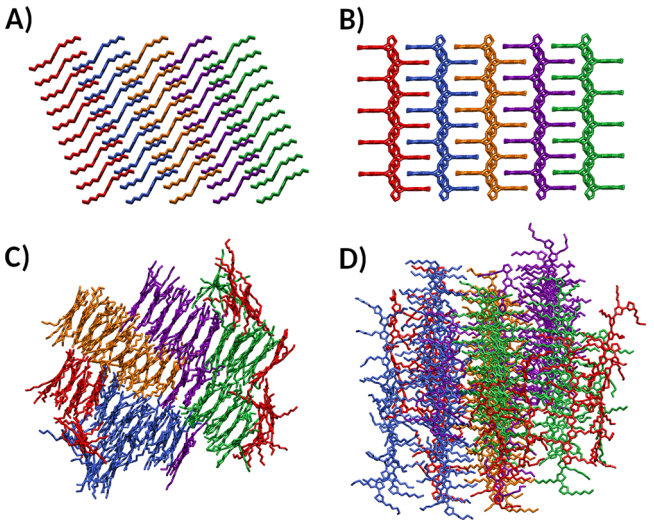

Figure 6. Snapshots of $(3HT)_{10}$ at 300 K using the BHA FF: (A) starting form II structure (view along the *b*-axis); (B) starting form II structure (view over the *ac*-plane); (C) final structure obtained after the transition to form I, cooled at 300 K (view along the *b*-axis); (D) final structure obtained after the transition to form I, cooled at 300 K (view over the *ac*-plane). The original form II and final from I stacking organization are highlighted, with chains color coding according to the initial form II stacking.

As compared to $(3HT)_{10}$, for both $(3HT)_{16}$ and $(3HT)_{20}$ the increase of the form II melting temperatures is with FF3 and OPL roughly consistent with the increase observed experimentally. MD recrystallization into form I crystals from the isotropic melt is a slow process, unlikely to be observed in our atomistic simulations, and was not attempted here. We note in passing that to observe successfully crystal nucleation in simulations, even in the case of polyethylene, where it is likely to be comparatively rapid, it was necessary to adopt united-atom force fields and input structures of large size.[73]

On the other hand, unsurprisingly, with the BHA force field the form II structure converts to a form I type structure also in the cases of $(3HT)_{16}$ and $(3HT)_{20}$, (see Table 3), exactly at the same temperature observed for both $(3HT)_{10}$ and for P3HT, with a crystal-to-crystal transformation mechanism closely similar to that shown for $(3HT)_{10}$ in Figure 6.

Form II P3HT and $(3HT)_n$ Structural Evolution and Thermodynamics. In Tables 3 and 4 we highlight the main thermodynamic features of the transitions observed heating form II of the investigated molecular systems. Because data are normalized by the number of monomer units, minor, regular variations are expected for the thermodynamic quantities characterizing a given transition and force field, as the degree of polymerization (DP) increases, plausibly approaching asymptotically polymer values for the same transition. The experimental form II P3HT melting enthalpy (Table 4) is, however, clearly higher than the value estimated for oligomers. This could be explained by the fact that while values for the polymer were obtained extrapolating to 100% crystallinity and infinite crystal size, the crystallinity of the oligomers' samples may well be 10−20% lower than the assumed 100% value. This possibility is supported by the fact (see above) that reflections indexed as form II 010 (corresponding to 001 according to the convention generally adopted[30]) show experimental spacings that are 10−20% larger than expected on the basis of the molecular length and actually observed in form I crystal structures.[30] Such reflections are actually broader and never show second or third orders, suggesting that they could possibly result from the alternation of crystalline and essentially amorphous layers. Terminal units, and associated disorder, could in principle also have destabilizing effects in experimental oligomer crystals.

The melting enthalpy per monomer unit of form II remains essentially constant with DP for oligomers both in the case of experimental values and for FF3, with variations of less than 10% within a given series (Table 4). For the OPL force field, larger form II melting enthalpy variations occur, increasing significantly with the DP. The absolute values of the form II melting enthalpies are about 20% larger than the experimental values in the case of FF3, while for OPL they are much larger (by about 80%), plausibly being the main cause leading to even more important deviations from the experimental form II melting temperatures.

It is important to note that in Table 3 all values reported, specifically also for the BHA force field, pertain to the form II−form I transition. Both enthalpy and entropy values are therefore expected to be substantially smaller than those of the from II isotropization observed for the oligomers with the other two force fields, which are reported in Table 4. Encouragingly, the variation of the form II−form I BHA transition enthalpy with DP is modest, but comparisons in Table 3 show them to be on average nearly twice the experimental values, likely substantially increasing the form II−form I transition temperature resulting from simulations with the BHA force field and also for the other two investigated force fields.

https://doi.org/10.1021/acs.macromol.2c00131
Macromolecules 2022, 55, 2398−2412

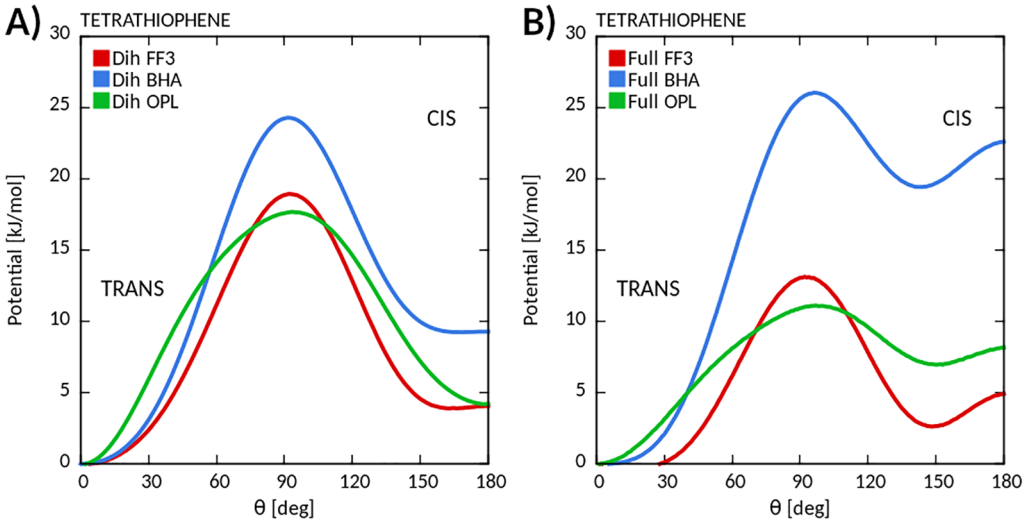

Figure 7. Dihedral (A) and full (B) potential profiles for the S−C−C−S bond in tetrathiophene.

Both the form II experimental melting entropy (Table 4) and the form II−form I transition entropy (Table 3) decrease with increasing DP: this is intuitively acceptable considering that larger ΔS values are expected for terminal units than for internal units. A qualitative understanding of the transition thermodynamics we are discussing can also be obtained considering[38] that as the DP increases, the entropy per monomer unit of the melt should and experimentally does decrease more than the entropy of the highly disordered form I (which can essentially be considered a mesophase). The entropy of form I will in turn decrease more than that of the much more ordered from II, whose entropy per monomer unit may, in first approximation, be considered invariant with DP. This behavior is qualitatively reproduced with FF3 for which (Table 4) isotropization ΔS decreases somewhat as DP increases, while surprisingly the form II isotropization entropy per monomer unit appears to significantly increase with DP using the OPL force field. On the other hand, we observe that for both FF3 and OPL, the isotropization ΔS values estimated from the calculations reasonably correspond with the experimental, somewhat larger deviations occurring in the case of $(3HT)_{20}$ treated with the OPL force field.

To help rationalize the results we just discussed, we extracted from the simulation results the contributions of intra- and intermolecular interactions to the internal energy changes (ΔU) which closely mirrors the enthalpy changes, during form II phase transitions. Only two contributions were found to change significantly during the transitions we are examining. These two terms, associated with the dihedral angle potential (ΔU_{dih}) and with the Lennard-Jones short-range interactions ($\Delta U_{L\text{-}J}$), are collected in the Supporting Information (Table S8). The estimate of these terms was addressed by using the fitting procedure described above for the enthalpy. We note that due to numerical fluctuations of the internal energy in the simulation runs, the sum of these two terms may exceed by about 10% the total transition enthalpies in Table 3, while it may be smaller because of other terms contributing to the transition enthalpy. Our discussion will hence be essentially qualitative.

The magnitude of the $\Delta U_{L\text{-}J}$ terms varies for oligomers quite significantly with different force fields, despite the fact that similar parameters, essentially borrowed from the OPLS parameter set, were used to describe nonbonded interactions. We note that the term is smaller for FF3 than for the other two force fields and quite clearly so with respect to OPL. Differences are somewhat less important between FF3 and BHA, but the latter involves form II−form I conversions which should involve lower potential energy differences than the isotropization transitions. The $\Delta U_{L\text{-}J}$ terms are much more similar in the case of the P3HT polymer, for which all the three force fields predict a form II−form I transition, in which the loss of side-chain interdigitation is certainly a key factor. To verify this hypothesis, the contributions associated with hexyl side-chain atoms ($-C_6H_{13}$) were identified. The analysis of these results confirmed that the largest fraction of $\Delta U_{L\text{-}J}$ (up to 90%) was associated with the loss of alkyl side-chain packing during the melting process. Both in the case of FF3 and OPL it is possible to compare the $\Delta U_{L\text{-}J}$ terms for the form II melting transition occurring in oligomers, with the same term for the form II−form I transition occurring in polymers: quite reasonably the $\Delta U_{L\text{-}J}$ terms are overall somewhat higher in the isotropization transition.

The second significant contribution to the internal energy change occurring in the transitions we are examining is found to be associated with the dihedral angle potential U_{dih}. The terms ΔU_{dih} collect all contributions from the dihedral angles described by a specific potential function (the Rickaert−Belleman function, in the present case). It is apparent that for FF3 the ΔU_{dih} and $\Delta U_{L\text{-}J}$ contributions to a given transition are very similar both for all oligomer and polymer transformations. OPL shows a behavior similar to FF3 for oligomer form II melting, whereas in the case of the P3HT polymer form II−form I transition ΔU_{dih} is clearly smaller than $\Delta U_{L\text{-}J}$, similarly to what we find in all cases for BHA (form II−form I transformation in all cases), for which ΔU_{dih} is always clearly smaller and becomes negligible in the case of P3HT suggesting stiffer dihedral potential functions than the other two force fields.

We attempted to further detail our analysis separating the contributions due respectively to main chain and side chain dihedrals. In the first set, only the dihedrals containing the carbon atoms linking consecutive monomer units were considered, whereas, for the alkyl side chains, the analysis was restricted to the dihedrals strictly belonging to the hexyl

https://doi.org/10.1021/acs.macromol.2c00131
Macromolecules 2022, 55, 2398−2412

chains. For FF3 and OPL similar behaviors were observed. The relative contribution related to the side chain dihedrals increased, for form II melting, with the oligomer length, possibly due to some cooperative mechanism, enhanced by growing DP. For the corresponding polymers (form II−form I transition), the contribution associated with the main-chain dihedrals was essentially negligible, as expected, considering the additional constraint imposed by the periodic boundary conditions along the main-chain axis and the fact that the two forms have closely similar chain axis periodicity. For the BHA force field, (form II−form I transition) the contribution of the main-chain dihedrals was small or negligible in all cases, regardless of the oligomer length, further supporting and orienting the suggestion of potential function-dependent chain stiffness. To test this notion, we calculated for the three force fields the dihedral and the full (comprehensive of nonbonded interactions) potential for the tetrathiophene molecule by varying the central S−C−C−S torsional angle. In practice, the calculation was performed by gradually rotating half of the molecule along the bond connecting the two central atoms, so as to cover the range from 0°, corresponding to the *trans* conformation, to 180°, corresponding to the *cis* conformation. Bond lengths and angles were kept fixed during the rotation.

The result of this calculation, performed with Gromacs,[58−60] is shown in Figure 7. All full potential profiles show two energy basins, with minima located at 0° (i.e., the *trans* conformation) and slightly below 150°, the latter corresponding to a *cisoid* conformation already observed in our previous calculations.[39] The height of the barrier separating the two basins is similar for FF3 (13 kJ/mol) and OPL (11 kJ/mol), while for BHA a much higher value was found (27 kJ/mol), resulting in a steeper potential curve. The relative energy of the *cisoid* minimum with respect to *trans* considering the full potential (3 kJ/mol for FF3, 7 kJ/mol for OPL, and 19 kJ/mol for BHA) are also relevant. These features, and specifically the increased main-chain stiffness, are bound to play a significant role with respect to the thermal behavior observed with the BHA force field, promoting the form II transition to the mesomorphic form I in all oligomers, in essence broadening the thermodynamic stability range of this phase with respect to both the amorphous phase and the crystalline form II.

Increasing the main-chain conformational rigidity is also likely to play an essential role augmenting the melting points of form II, but plausibly less so than for form I, as estimated by MD simulations.

The fact that the BHA force field affords readily form I type structural models in the case of all the studied oligomers allowed us to explore the thermal stability of structural models derived from these structures also with the other two force fields. Form I models were hence built for $(3HT)_{10}$, $(3HT)_{16}$, and $(3HT)_{20}$ from the coordinates of the corresponding BHA oligomers, cooled at 300 K. The resulting structures were then heated at their form II isotropization temperatures reported in Table 4 for 40 ns runs, adopting however the FF3 and the OPL force fields.

We were hence able to check if form I like structures are predicted to be stable at the temperature where form II melts, and this was indeed the case for $(3HT)_{16}$ and $(3HT)_{20}$, but not for $(3HT)_{10}$ using the FF3 force field. This result indicates that whereas a form II−form I solid−solid transition is not viable, melting of form II and recrystallization into form I is compatible in the case of FF3 with our simulations in the case of $(3HT)_{16}$ and $(3HT)_{20}$. Surprisingly, in the case of the OPL force field derived models, form I was found to melt just below the melting point of form II in the case of all three investigated oligomers.

CONCLUSIONS

In the present work we were able to show that the P3HT polymer form II crystal structure is a clearly identifiable potential energy minimum not only with the FF3 force field we used in previous work[39] but also with the other two thiophene specific force fields (BHA and OPL) we chose to investigate. The same form II potential energy minimum is also identified by solid-state DFT calculations. Similar conclusions with the three force fields and with DFT calculations were reached considering the form II $(3HT)_n$ oligomers crystal structures, which can be extrapolated from the polymer crystal structures and from the published experimental work, for form II $(3HT)_n$ oligomer crystals.[30,32] These structures were the starting point to investigate by molecular dynamics with the three force fields FF3, BHA, and OPL the changes and phase transitions induced by increasing temperature and compare our results with the available experimental data.[30] The main results of these simulations are presented synoptically in Figure 8 and can be summarized as follows.

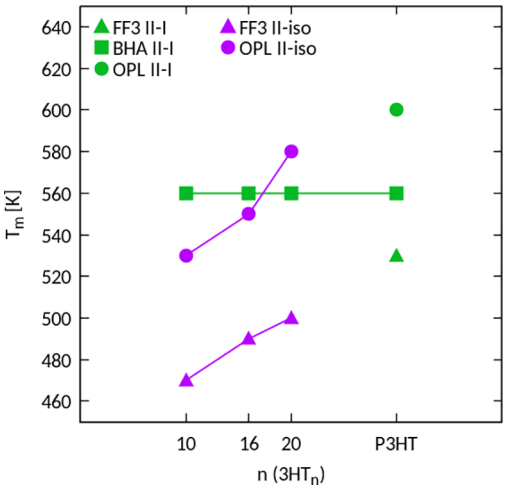

Figure 8. Form II disordering transitions temperatures resulting from the MD simulations for each of the force fields considered as a function of the degree of polymerization *n*. With the BHA force field, the form II−form I transition rather than form II isotropization is observed for all the investigated molecular systems, at about 560 K.

All three investigated force fields predict a solid−solid, or better a solid−mesophase, form II−form I transition for P3HT polymers. In all cases, the transition occurs through a preliminary substantial disordering, high-energy stage which is followed by rapid re-establishment of optimal stacking of the main chains and improvement of the packing energy. The obtained form I shows, in all cases, features that are described more appropriately as mesomorphic rather than 3D crystalline (see Figure 4 and ref 39). Although the transition temperatures are substantially higher than those reported experimentally, this outcome is encouraging and indicates that all the force fields qualitatively capture the experimentally observed transition between the two forms.

As shown in Figure 8, investigation of selected oligomer systems (i.e., $(3HT)_{10}$, $(3HT)_{16}$, and $(3HT)_{20}$) yields results that more significantly differ, depending on the adopted force

https://doi.org/10.1021/acs.macromol.2c00131
Macromolecules 2022, 55, 2398−2412

field. Two force fields, namely FF3 and OPL, which appear to give results that are somewhat more reliable, imply that a melting−recrystallization process is likely to occur for oligomers, which corresponds to the indications resulting from the experimental diffraction investigation on oligomers.[30] For the BHA, conversely, a mechanism leading, at least initially, to a form I showing features of a highly disordered nematic, applies to all oligomers investigated.

As for P3HT, the transition temperatures are higher than those expected based on the available data. The overestimation is similar to OPL (190−210 K) and with BHA (180−210 K). With the BHA force field, however, an additional qualitative deviation from experimental data results, as the transition temperature is surprisingly invariant, and form II transforms into form I at 560 K, irrespective of the DP of the molecular system. Adopting OPL and FF3, on the other hand, the transition, occurring in the simulations of the oligomers we studied, was the form II melting. In the case of FF3 the overestimation of the transition temperature is somewhat more moderate and decreases from 140 K in the case of the polymer to 120−130 K for the oligomers. We shall return to this point below.

Experimentally[30] (see Figure 1), form II is found to have a higher melting point than form I for $(3HT)_n$ oligomers up to n = 12, whereas the high-entropy form I becomes the higher melting point polymorph for $n > 12$. This "crossover", degree-of-polymerization-dependent behavior qualitatively mirrors what has been described by various authors for oligomer systems displaying mesomorphic phases along with a crystalline phase.[38] The stability of the mesophase with respect to the melt is bound to decrease as the DP decreases, especially so with systems with moderate chain rigidity, due to the role of terminal units. Form I for $(3HT)_n$ with $n < 13$ becomes experimentally a metastable monotropic phase that may be obtained only cooling from the melt and which transforms to the stable form II upon heating. Even a qualitative reproduction by MD simulations of this DP-dependent behavior appears to be a very challenging and significant force-field test. This corresponds to our observations with FF3: adopting this force field, the melting temperature of form I for $(3HT)_{10}$ turned out to be about 20 K lower than for form II (see the final part of the discussion), whereas form I is clearly the higher melting point polymorph for $(3HT)_{16}$.

With the OPL force field, form II is clearly the more stable, higher melting phase in the case of $(3HT)_{10}$, while form II and form I appear to have about the same melting point, close to 550 K for $(3HT)_{16}$ and to 580 K for $(3HT)_{20}$. In the case of infinite P3HT, on the other hand, form II transforms with OPL into a well-organized form I (Figure 4D) at high temperature (600 K). The results obtained with the BHA force field imply that with this choice, for all the studied molecular systems, form II is the more stable form at low temperature, whereas form I has, irrespective of DP, a higher melting point and becomes the more stable phase at high temperature plausibly because of the high main-chain rigidity.

The comparison of different force fields allows to evidence molecular factors responsible for the stability of a given polymorph for different oligomer lengths in $(3HT)_n$ systems: while OPL, the force field showing consistently the higher transition enthalpies (see Tables 3 and 4), expands the crystalline form II stability range at the expenses of both form I and the melt, the force field (BHA) with highest chain rigidity (see Figure 7) expands the temperature stability window of the mesomorphic form I. Indeed, the high main-chain rigidity is plausibly the factor leading to the mentioned essentially identical behavior of all studied oligomers and the polymer observed in our simulations with the BHA force field. Quite obviously a high main-chain rigidity stabilizes also the well-ordered crystalline form II, but less so than the high-entropy form I. Somewhat more balanced estimates and predictions are obtained with FF3 which apparently manages to strike a better compromise between the different key force-field parameters, possibly because it was optimized to reproduce crystalline packings of alkylthiophene-based oligomers and polymers.

As mentioned above, all the force fields overestimate the transition temperatures in both polymers and oligomers. This outcome is due to a number of different factors. To keep our systems at a manageable size and complexity, we adopted highly ordered starting input structures, which are likely to represent a rather extreme idealization of experimental samples of crystalline conjugated polymers and oligomers.[74−76] Indeed, the small experimental crystal size and the widespread presence of defects, of disorder, and of strained amorphous regions surrounding the crystalline domains can reasonably be expected to lower the transition temperatures, thereby contributing to the explanation of the observed outcomes.

Other factors can be related to the force field parametrization. As shown by our simulations, differences in FF parametrization may significantly affect the predicted thermal behavior of P3HT and its oligomers. At the core of such difficulty is the existence of competing, complex intra- and intermolecular interactions, which are intrinsically at the limits of molecular mechanics approaches.

All the force fields adopted in this work were developed starting from the OPLS parametrization. The parameters describing the dispersive interactions were closely similar across the different force fields, whereas we found major differences in the atomic charges which are adopted also in efforts to overcome the intrinsic limitations of force fields with respect to intra- and intermolecular interactions resulting from delocalized π electrons. Because of the long-range nature of the electrostatic potential, the balance between atomic charges may well affect packing energies, generally resulting in perturbed transition temperatures. Other additional FF-specific factors, such as the degree of conformational stiffness of the main chain for the BHA force field, may have also contributed to the above observed differences in the oligomer's thermal behavior.

If, on one side, improvements should be addressed to more precisely reproduce the behavior of 3-alkylthiophenes, on the other hand, significant efforts should also be devoted to assessing force field and more in general simulations' reliability and limits.[77] The latter task may greatly benefit from the application of quantum mechanical approaches, such as solid-state DFT, which, thanks to highly parallel implementations, can now be successfully applied to systems comprising hundreds of atoms[78,79] albeit for simulation times still well below than 1 ns.[80]

Meanwhile, some encouraging and positive messages emerge along with problematic issues from the present work. The above discussion evidence the ability of molecular dynamics to capture and predict trends and qualitative molecular behavior of 3-alkylthiophene polymers and oligomers to a very promising, force-field-dependent degree. Well-defined crystalline polymorphs like form II P3HT can be modeled successfully with different force fields, whereas simulations of

https://doi.org/10.1021/acs.macromol.2c00131
Macromolecules 2022, 55, 2398−2412

highly disordered structures like form I P3HT remain very challenging, and the developed structural models turn out to be highly force-field-dependent (see Figures 4 and 6). Our results suggest that similar approaches and considerations can also be extended to a large number of conjugated polymers characterized by the existence of different polymorphs, likely characterized by different degrees of side-chain interdigitation, the case of higher melting phases by highly disordered side-chain structures.

The possibility to simulate phase transitions allows to generate structures to be used to investigate disordered polymorphs models otherwise hardly accessible. This applies particularly to form I P3ATs and to similarly disordered structures. Our future efforts will be devoted to an improved, more detailed characterization of form I P3ATs with the aim at gaining a better understanding of their disorder features and thermal behavior.

■ ASSOCIATED CONTENT

Supporting Information

The Supporting Information is available free of charge at https://pubs.acs.org/doi/10.1021/acs.macromol.2c00131.

Summary of force field atom type assignments; supplementary tables with cell parameters, transition temperatures, internal energies, and DFT results (PDF)

■ AUTHOR INFORMATION

Corresponding Authors

Mosè Casalegno − *Dipartimento di Chimica, Materiali e Ingegneria Chimica "G. Natta", Politecnico di Milano, I-20131 Milano (MI), Italy;* orcid.org/0000-0002-4833-2990; Email: mose.casalegno@polimi.it

Stefano Valdo Meille − *Dipartimento di Chimica, Materiali e Ingegneria Chimica "G. Natta", Politecnico di Milano, I-20131 Milano (MI), Italy;* orcid.org/0000-0003-3071-6651; Email: valdo.meille@polimi.it

Author

Antonino Famulari − *Dipartimento di Chimica, Materiali e Ingegneria Chimica "G. Natta", Politecnico di Milano, I-20131 Milano (MI), Italy*

Complete contact information is available at: https://pubs.acs.org/10.1021/acs.macromol.2c00131

Notes

The authors declare no competing financial interest.

■ ACKNOWLEDGMENTS

The authors thank and acknowledge Prof. Martin Heeney for allowing and providing access to original data from ref 30 and Prof. Guido Raos for stimulating ongoing discussions. The authors acknowledge the CINECA award under the ISCRA initiative (project POLYMOTH, n. HP10C8HAC6) for the availability of high-performance computing resources and support.

■ REFERENCES

(1) Hedley, G. J.; Ruseckas, A.; Samuel, I. D. W. Light Harvesting for Organic Photovoltaics. *Chem. Rev.* **2017**, *117*, 796.

(2) Root, S. E.; Savagatrup, S.; Printz, A. D.; Rodriquez, D.; Lipomi, D. J. Mechanical Properties of Organic Semiconductors for Stretchable, Highly Flexible, and Mechanically Robust Electronics. *Chem. Rev.* **2017**, *117* (9), 6467−6499.

(3) Ostroverkhova, O. Organic Optoelectronic Materials: Mechanisms and Applications. *Chem. Rev.* **2016**, *116*, 13279.

(4) Sirringhaus, H.; Brown, P.; Friend, R.; Nielsen, M. M.; Bechgaard, K.; Langeveld-Voss, B. M. W.; Spiering, A. J. H.; Janssen, R. A. J.; Meijer, E. W.; Herwig, P.; de Leeuw, D. M. Two-dimensional charge transport in self-organized, high-mobility conjugated polymers. *Nature* **1999**, *401*, 685−688.

(5) Sirringhaus, H.; Tessler, N.; Friend, R. Integrated Optoelectronic Devices Based on Conjugated Polymers. *Science* **1998**, *280*, 1741−1744.

(6) Bao, Z.; Dodabalapur, A.; Lovinger, A. J. Soluble and processable regioregular poly(3-hexylthio-phene) for thin film field-effect transistor applications with high mobility. *Appl. Phys. Lett.* **1996**, *69*, 4108−4110.

(7) Lu, L.; Zheng, T.; Wu, Q.; Schneider, A. M.; Zhao, D.; Yu, L. Recent Advances in Bulk Heterojunction Polymer Solar Cells. *Chem. Rev.* **2015**, *115* (23), 12666−12731.

(8) Dang, M. T.; Hirsch, L.; Wantz, G.; Wuest, J. D. Controlling the Morphology and Performance of Bulk Heterojunctions in Solar Cells. Lessons Learned from the Benchmark Poly(3-hexylthiophene):[6,6]-Phenyl-C61-butyric Acid Methyl Ester System. *Chem. Rev.* **2013**, *113*, 3734−3765.

(9) Heremans, P.; Cheyns, D.; Rand, B. P. Strategies for Increasing the Efficiency of Heterojunction Organic Solar Cells: Material Selection and Device Architecture. *Acc. Chem. Res.* **2009**, *42* (11), 1740−1747.

(10) Wang, C.; Dong, H.; Hu, W.; Liu, Y.; Zhu, D. Semiconducting π-Conjugated Systems in Field-Effect Transistors: A Material Odyssey of Organic Electronics. *Chem. Rev.* **2012**, *112*, 2208−2267.

(11) Janasz, L.; Chlebosz, D.; Gradzka, M.; Zajaczkowski, W.; Marszalek, T.; Müllen, K.; Ulanski, J.; Kiersnowski, A.; Pisula, W. Improved charge carrier transport in ultrathin poly(3-hexylthiophene) films via solution aggregation. *J. Mater. Chem. C* **2016**, *4*, 11488−11498.

(12) Jang, M.; Huh, Y.; Chang, M. Effects of Solvent Vapor Annealing on Morphology and Charge Transport of Poly(3-hexylthiophene) (P3HT) Films Incorporated with Preformed P3HT Nanowires. *Polymers* **2020**, *12* (5), 1188.

(13) Kline, R. J.; McGehee, M. D.; Kadnikova, E.; Liu, J.; Fréchet, J. M. J. Controlling the Field-Effect Mobility of Regioregular Polythiophene by Changing the Molecular Weight. *Adv. Mater.* **2003**, *15*, 1519−1522.

(14) O'Connor, B.; Reid, O. G.; Zhang, X.; Kline, R. J.; Richter, L. J.; Gundlach, D. J.; DeLongchamp, D. M.; Toney, M. F.; Kopidakis, N.; Rumbles, G. Morphological Origin of Charge Transport Anisotropy in Aligned Polythiophene Thin Films. *Adv. Funct. Mater.* **2014**, *24*, 3422−3431.

(15) Pingel, P.; Zen, A.; Abellon, R. D.; Grozema, F. C.; Siebbeles, L. D. A.; Neher. Temperature-Resolved Local and Macroscopic Charge Carrier Transport in Thin P3HT Layers. D. *Adv. Funct. Mater.* **2010**, *20*, 2286−2295.

(16) Kline, R. J.; McGehee, M. D.; Kadnikova, E. N.; Liu, J.; Fréchet, J. M. J.; Toney, M. F. Dependence of Regioregular Poly(3-hexylthiophene) Film Morphology and Field-Effect Mobility on Molecular Weight. *Macromolecules* **2005**, *38* (8), 3312−3319.

(17) Gutt, C.; Grodd, L.; Mikayelyan, E.; Pietsch, U.; Kline, R. J.; Grigorian, S. Local Orientational Structure of a P3HT π−π Conjugated Network Investigated by X-ray Nanodiffraction. *J. Phys. Chem. Lett.* **2014**, *5*, 2335−2339.

(18) Nieuwendaal, R. C.; Snyder, C. R.; DeLongchamp, D. M. Measuring Order in Regioregular Poly(3-hexylthiophene) with Solid-State 13 C CPMAS NMR. *ACS Macro Lett.* **2014**, *3* (2), 130−135.

(19) Persson, N. E.; Chu, P.-H.; McBride, M.; Grover, M.; Reichmanis, E. Nucleation, Growth, and Alignment of Poly(3-hexylthiophene) Nanofibers for High-Performance OFETs. *Acc. Chem. Res.* **2017**, *50*, 932−942.

(20) Snyder, C. R.; Nieuwendaal, R. C.; DeLongchamp, D. M.; Luscombe, C. K.; Sista, P.; Boyd, S. D. Quantifying Crystallinity in High Molar Mass Poly(3-hexylthiophene). *Macromolecules* **2014**, *47*, 3942−3950.
(21) Brinkmann, M.; Rannou, P. Effect of Molecular Weight on the Structure and Morphology of Oriented Thin Films of Regioregular Poly(3-hexylthiophene) Grown by Directional Epitaxial Solidification. *Adv. Funct. Mater.* **2007**, *17*, 101−108.
(22) Panzer, F.; Bässler, H.; Lohwasser, R.; Thelakkat, M.; Köhler, A. The Impact of Polydispersity and Molecular Weight on the Order-Disorder Transition in Poly(3-hexylthiophene). *J. Phys. Chem. Lett.* **2014**, *5*, 2742−2747.
(23) Brinkmann, M. Structure and Morphology Control in Thin Films of Regioregular Poly(3-hexylthiophene). *J. Polym. Sci., Part B: Polym. Phys.* **2011**, *49*, 1218−1233.
(24) Liu, J.; Arif, M.; Zou, J.; Khondaker, S. I.; Zhai, L. Controlling Poly(3-hexylthiophene) Crystal Dimension: Nanowhiskers and Nanoribbons. *Macromolecules* **2009**, *42*, 9390−9393.
(25) Prosa, T. J.; Winokur, M. J.; Moulton, J.; Smith, P.; Heeger, A. J. X-ray Structural Studies of Poly(3-alkylthiophenes): An Example of an Inverse Comb. *Macromolecules* **1992**, *25*, 4364−4372.
(26) Prosa, T. J.; Winokur, M. J.; McCullough, R. D. Evidence of a Novel Side Chain Structure in Regioregular Poly(3-alkylthiophenes). *Macromolecules* **1996**, *29*, 3654−3656.
(27) Buono, A.; Son, N. H.; Raos, G.; Gila, L.; Cominetti, A.; Catellani, M.; Meille, S. V. Form II Poly(3-butylthiophene): Crystal Structure and Preferred Orientation in Spherulitic Thin Films. *Macromolecules* **2010**, *43*, 6772−6781.
(28) Guilbert, A. A. Y.; Urbina, A.; Abad, J.; Díaz-Paniagua, C.; Batallán, F.; Seydel, T.; Zbiri, M.; García-Sakai, V.; Nelson, J. Temperature-Dependent Dynamics of Polyalkylthiophene Conjugated Polymers: A Combined Neutron Scattering and Simulation Study. *Chem. Mater.* **2015**, *27* (22), 7652−7661.
(29) Koch, F. P. V.; Smith, P.; Heeney, M. Fibonacci's Route" to Regioregular Oligo(3-hexylthiophene)s. *J. Am. Chem. Soc.* **2013**, *135* (37), 13695−13698.
(30) Koch, F. P. V.; Heeney, M.; Smith, P. Thermal and Structural Characteristics of Oligo(3-hexylthiophene)s (3HT)n, n = 4−36. *J. Am. Chem. Soc.* **2013**, *135*, 13699.
(31) Koch, F. P. V.; Rivnay, J.; Foster, S.; Muller, C.; Downing, J. M.; Buchaca-Domingo, E.; Westacott, P.; Yu, L.; Yuan, M.; Baklar, M.; Fei, Z.; Luscombe, C.; McLachlan, M. A.; Heeney, M.; Rumbles, G.; Silva, C.; Salleo, A.; Nelson, J.; Smith, P.; Stingelin, N. The impact of molecular weight on microstructure and charge transport in semicrystalline polymer semiconductors−poly(3-hexylthiophene), a model study. *Prog. Polym. Sci.* **2013**, *38*, 1978−1989.
(32) Rahimi, K.; Botiz, I.; Stingelin, N.; Kayunkid, N.; Sommer, M.; Koch, F. P. V.; Nguyen, H.; Coulembier, O.; Dubois, P.; Brinkmann, M.; Reiter, G. Controllable Processes for Generating Large Single Crystals of Poly(3-hexylthiophene). *Angew. Chem., Int. Ed.* **2012**, *51*, 11131−11135.
(33) Brambilla, L.; Tommasini, M.; Botiz, I.; Rahimi, K.; Agumba, J. O.; Stingelin, N.; Zerbi, G. Regio-Regular Oligo and Poly(3-hexyl thiophene): Precise Structural Markers from the Vibrational Spectra of Oligomer Single Crystals. *Macromolecules* **2014**, *47* (19), 6730−6739.
(34) Joshi, S.; Grigorian, S.; Pietsch, U. X-ray structural and crystallinity studies of low and high molecular weight poly(3-hexylthiophene). *Phys. Stat. Sol. (a)* **2008**, *205* (3), 488−496.
(35) Lu, G.; Li, L.; Yang, X. Achieving Perpendicular Alignment of Rigid Polythiophene Backbones to the Substrate by Using Solvent-Vapor Treatment. *Adv. Mater.* **2007**, *19*, 3594−3598.
(36) Lu, G.; Li, L.; Yang, X. Morphology and Crystalline Transition of Poly(3-butylthiophene) Associated with Its Polymorphic Modifications. *Macromolecules* **2008**, *41*, 2062−2070.
(37) Yuan, Y.; Zhang, J.; Sun, J. Effect of Solvent Evaporation Rate on Order-to-Disorder Phase Transition Behavior of Regioregular Poly(3-butylthiophene). *Macromolecules* **2011**, *44*, 6128−6135.
(38) Percec, V.; Keller, A. A Thermodynamic Interpretation of Polymer Molecular Weight Effect on the Phase Transitions of Main-Chain and Side-Chain Liquid-Crystal Polymers. *Macromolecules* **1990**, *23*, 4347−4350.
(39) Casalegno, M.; Nicolini, T.; Famulari, A.; Raos, G.; Po, R.; Meille, S. V. Atomistic modelling of entropy driven phase transitions between different crystal modifications in polymers: the case of poly(3-alkylthiophenes). *Phys. Chem. Chem. Phys.* **2018**, *20*, 28984−28989.
(40) Moreno, M.; Casalegno, M.; Raos, G.; Meille, S. V.; Po, R. Molecular Modeling of Crystalline Alkylthiophene Oligomers and Polymers. *J. Phys. Chem. B* **2010**, *114*, 1591−1602.
(41) Raos, G.; Famulari, A.; Marcon, V. Computational reinvestigation of the bithiophene torsion potential. *Chem. Phys. Lett.* **2003**, *379*, 364−372.
(42) Bhatta, R. S.; Yimer, Y. Y.; Perry, D. S.; Tsige, M. Improved Force Field for Molecular Modeling of Poly(3-hexylthiophene). *J. Phys. Chem. B* **2013**, *117*, 10035−10045.
(43) Bhatta, R. S.; Yimer, Y. Y.; Tsige, M.; Perry, D. S. Conformations and torsional potentials of poly(3-hexylthiophene) oligomers: Density functional calculations up to the dodecamer. *Comput. Theor. Chem.* **2012**, *995*, 36−42.
(44) Wildman, J.; Repiščák, P.; Paterson, M. J.; Galbraith, I. General Force-Field Parametrization Scheme for Molecular Dynamics Simulations of Conjugated Materials in Solution. *J. Chem. Theory Comput.* **2016**, *12*, 3813−3824.
(45) Wolf, C. M.; Kanekal, K. H.; Yimer, Y. Y.; Tyagi, M.; Omar-Diallo, S.; Pakhnyuk, V.; Luscombe, C. K.; Pfaendtner, J.; Pozzo, L. D. Assessment of molecular dynamics simulations for amorphous poly (3-hexylthiophene) using neutron and X-ray scattering experiments. *Soft Matter* **2019**, *15*, 5067−5083.
(46) Oostenbrink, C.; Villa, A.; Mark, A. E.; van Gunsteren, W. F. A biomolecular force field based on the free enthalpy of hydration and solvation: The GROMOS force-field parameter sets 53A5 and 53A6. *J. Comput. Chem.* **2004**, *25*, 1656−1676.
(47) Wang, J.; Wolf, R. M.; Caldwell, J. W.; Kollman, P. A.; Case, D. A. Development and Testing of a General Amber Force Field. *J. Comput. Chem.* **2004**, *25*, 1157−1174.
(48) Jorgensen, W. L.; McDonald, N. A. Development of an All-Atom Force Field for Heterocycles. Properties of Liquid Pyridine and Diazenes. *J. Mol. Struct.: THEOCHEM* **1998**, *424*, 145.
(49) Rizzo, R. C.; Jorgensen, W. L. OPLS All-Atom Model for Amines: Resolution of the Amine Hydration Problem. *J. Am. Chem. Soc.* **1999**, *121* (20), 4827−4836.
(50) Jorgensen, W. L.; McDonald, N. A. Development of an All-Atom Force Field for Heterocycles. Properties of Liquid Pyridine and Diazenes. *J. Mol. Struct.: THEOCHEM* **1998**, *424*, 145−155.
(51) Jorgensen, W. L.; Maxwell, D. S.; Tirado-Rives, J. Development and Testing of the OPLS All-Atom Force Field on Conformational Energetics and Properties of Organic Liquids. *J. Am. Chem. Soc.* **1996**, *118* (45), 11225−11236.
(52) Schwarz, K. N.; Kee, T. W.; Huang, D. M. Coarse-Grained Simulations of the Solution-Phase Self-Assembly of Poly(3-Hexylthiophene) Nanostructures. *Nanoscale* **2013**, *5* (5), 2017−2027.
(53) Huang, D. M.; Moule, A. J.; Faller, R. Characterization of Polymer-Fullerene Mixtures for Organic Photovoltaics by Systematically Coarse-Grained Molecular Simulations. *Fluid Phase Equilib.* **2011**, *302* (1−2), 21−25.
(54) Dubay, K. H.; Hall, M. L.; Hughes, T. F.; Wu, C.; Reichman, D. R.; Friesner, R. A. Accurate Force Field Development for Modeling Conjugated Polymers. *J. Chem. Theory Comput.* **2012**, *8* (11), 4556−4569.
(55) Borzdun, N. I.; Larin, S. V.; Falkovich, S. G.; Nazarychev, V. M.; Volgin, I. V.; Yakimansky, A. V.; Lyulin, A. V.; Negi, V.; Bobbert, P. A.; Lyulin, S. V. Molecular dynamics simulation of poly(3-hexylthiophene) helical structure *In Vacuo* and in amorphous polymer surrounding. *J. Polym. Sci., Part B: Polym. Phys.* **2016**, *54*, 2448−2456.
(56) Bayly, C. I.; Cieplak, P.; Cornell, W. D.; Kollman, P. A. A Well-Behaved Electrostatic Potential Based Method Using Charge

https://doi.org/10.1021/acs.macromol.2c00131
Macromolecules 2022, 55, 2398−2412

Restraints for Deriving Atomic Charges: The RESP Model. *J. Phys. Chem.* **1993**, *97*, 10269−10280.
(57) Cornell, W. D.; Cieplak, P.; Bayly, C. I.; Kollman, P. A. Application of RESP Charges To Calculate Conformational Energies, Hydrogen Bond Energies, and Free Energies of Solvation. *J. Am. Chem. Soc.* **1993**, *115*, 9620−9631.
(58) Van Der Spoel, D.; Lindahl, E.; Hess, B.; Groenhof, G.; Mark, A. E.; Berendsen, H. J. C. (2005) GROMACS: Fast, flexible, and free. *J. Comput. Chem.* **2005**, *26*, 1701−1718.
(59) Berendsen, H. J. C.; van der Spoel, D.; van Drunen, R. GROMACS: A Message-passing Parallel Molecular Dynamics Implementation. *Comput. Phys. Commun.* **1995**, *91*, 43−56.
(60) Hess, B.; Kutzner, C.; van der Spoel, D.; Lindahl, E. GROMACS 4: Algorithms for Highly Efficient, Load-Balanced, and Scalable Molecular Simulation. *J. Chem. Theory Comput.* **2008**, *4* (3), 435−447.
(61) Bussi, G.; Donadio, D.; Parrinello, M. Canonical sampling through velocity rescaling. *J. Chem. Phys.* **2007**, *126*, 014101.
(62) Parrinello, M.; Rahman, A. Polymorphic transitions in single crystals: a new molecular dynamics method. *J. Appl. Phys.* **1981**, *52*, 7182−7190.
(63) Berendsen, H. J. C.; Postma, J. P. M.; van Gunsteren, W. F.; Di Nola, A.; Haak, J. R. Molecular dynamics with coupling to an external bath. *J. Chem. Phys.* **1984**, *81*, 3684−3690.
(64) Darden, T.; York, D.; Pedersen, L. Particle mesh Ewald: an Nlog(N) method for Ewald sums in large systems. *J. Chem. Phys.* **1993**, *98* (12), 10089−10092.
(65) Delley, B. From molecules to solids with the $DMol^3$ approach. *J. Chem. Phys.* **2000**, *113*, 7756−7764.
(66) Perdew, J. P.; Burke, K.; Ernzerhof, M. Generalized Gradient Approximation Made Simple. *Phys. Rev. Lett.* **1996**, *77* (18), 3865−3868.
(67) Perdew, J. P.; Burke, K.; Ernzerhof, M. Generalized Gradient Approximation Made Simple. *Phys. Rev. Lett.* **1997**, *78*, 1396. (Erratum).
(68) Tkatchenko, A.; Scheffler, M. Accurate molecular van der Waals interactions from ground-state electron density and free-atom reference data. *Phys. Rev. Lett.* **2009**, *102*, 073005.
(69) Baggioli, A.; Meille, S. V.; Raos, G.; Po, R.; Brinkmann, M.; Famulari, A. Intramolecular CH/π interactions in alkylaromatics: Monomer conformations for poly(3-alkylthiophene) atomistic models. *Int. J. Quantum Chem.* **2013**, *113*, 2154−2162.
(70) Humphrey, W.; Dalke, A.; Schulten, K. J. VMD: visual molecular dynamics. *Mol. Graphics* **1996**, *14*, 33−38.
(71) Gnuplot release 5.2. Thomas Williams and Colin Kelley. Gnuplot 4.6: An Interactive Plotting Program. http://sourceforge.net/projects/gnuplot (accessed 2021-07-26).
(72) Biovia Discovery Studio 2021, Dassault Systemes: 1233 Lujiazui Ring Road, Pudong, 200120 Shanghai, China. https://www.3ds.com/products-services/biovia (accessed 2021-07-26).
(73) Yi, P.; Locker, C. R.; Rutledge, G. C. Molecular Dynamics Simulation of Homogeneous Crystal Nucleation in Polyethylene. *Macromolecules* **2013**, *46* (11), 4723−4733.
(74) Wie, J. J.; Nguyen, N. A.; Cwalina, C. D.; Liu, J.; Martin, D. C.; Mackay, M. E. Shear-Induced Solution Crystallization of Poly(3-Hexylthiophene) (P3HT). *Macromolecules* **2014**, *47* (10), 3343−3349.
(75) Wu, Z.; Petzold, A.; Henze, T.; Thurn-Albrecht, T.; Lohwasser, R. H.; Sommer, M.; Thelakkat, M. Temperature and Molecular Weight Dependent Hierarchical Equilibrium Structures in Semiconducting Poly(3-Hexylthiophene). *Macromolecules* **2010**, *43* (10), 4646−4653.
(76) Liu, J.; Sun, Y.; Gao, X.; Xing, R.; Zheng, L.; Wu, S.; Geng, Y.; Han, Y. Oriented Poly(3-Hexylthiophene) Nanofibril with the π-π Stacking Growth Direction by Solvent Directional Evaporation. *Langmuir* **2011**, *27* (7), 4212−4219.
(77) Wolf, C. M.; Guio, L.; Scheiwiller, S.; Pakhnyuk, V.; Luscombe, C.; Pozzo, L. D. Strategies for the Development of Conjugated Polymer Molecular Dynamics Force Fields Validated with Neutron and X-Ray Scattering. *ACS Polym. Au* **2021**, *1* (3), 134−152.
(78) Ko, H.-Y.; Jia, J.; Santra, B.; Wu, X.; Car, R.; DiStasio, R. A., Jr. Enabling Large-Scale Condensed-Phase Hybrid Density Functional Theory Based Ab Initio Molecular Dynamics. 1. Theory, Algorithm, and Performance. *J. Chem. Theory Comput.* **2020**, *16* (6), 3757−3785.
(79) Ko, H. Y.; Santra, B.; Distasio, R. A. Enabling Large-Scale Condensed-Phase Hybrid Density Functional Theory-Based Ab Initio Molecular Dynamics II: Extensions to the Isobaric-Isoenthalpic and Isobaric-Isothermal Ensembles. *J. Chem. Theory Comput.* **2021**, *17* (12), 7789−7813.
(80) Raos, G.; Zappone, B. Polymer Adhesion: Seeking New Solutions for an Old Problem. *Macromolecules* **2021**, *54* (23), 10617−10644.

https://doi.org/10.1021/acs.macromol.2c00131
Macromolecules 2022, 55, 2398−2412